

Full two-photon downconversion of just a single photon

E. Sánchez-Burillo,¹ L. Martín-Moreno,¹ J. J. García-Ripoll,² and D. Zueco^{1,3}

¹*Instituto de Ciencia de Materiales de Aragon and Departamento de Física de la Materia Condensada, CSIC-Universidad de Zaragoza, E-50012 Zaragoza, Spain*

²*Instituto de Física Fundamental, IFF-CSIC, Calle Serrano 113b, Madrid E-28006, Spain*

³*Fundacion ARAID, Paseo Maria Agustín 36, E-50004 Zaragoza, Spain*

We demonstrate, both numerically and analytically, that it is possible to generate two photons from one and only one photon. We characterize the output two photon field and make our calculations close to reality by including losses. Our proposal relies on real or artificial three-level atoms with a cyclic transition strongly coupled to a one-dimensional waveguide. We show that close to perfect downconversion with efficiency over 99% is reachable using state-of-the-art Waveguide QED architectures such as photonic crystals or superconducting circuits. In particular, we sketch an implementation in circuit QED, where the three level atom is a transmon.

PACS numbers: 42.50.Ct, 42.50.Hz, 42.65.-k, 78.20.Bh

I. INTRODUCTION

The interaction between the electromagnetic field and quantum discrete level systems (like atoms) may be enhanced by confining light in one-dimensional waveguides [1–12]. In these setups, a key parameter is the ratio between the decay rate due to coupling to waveguide photons and that due to coupling to all other channels. Whenever the former dominates, we are in *strong coupling* regime of light-matter interactions. In this case, a single two-level system can not be only used to induce effective photon-photon interactions, but it also enables *minimal* and *highly efficient* optical devices, such as perfect mirrors [13–15], single photon lasing [16] and Raman scattering [17–19].

Another optical process that could strongly benefit from an enhanced light-matter interaction is photon downconversion, where a light beam of a given frequency is split into two beams whose frequencies add up to the original one. Downconversion is routinely used for the generation of entangled photons, and light at convenient frequencies. This is already done in atomic and molecular experiments and it could also be useful for energy harvesting, by using photons of high energy to excite more suitable transitions in a photovoltaic material. Photon down- and up-conversion are currently realized in bulk optics with the help of nonlinear noncentrosymmetric materials [20]. Moreover, due to the smallness of the fine structure constant, the typical performance of this process in crystals such as BBOs is very small, with only about one in every 10^{12} photons being downconverted [20].

A cyclic three level system (C3LS) strongly coupled to a waveguide is the *minimal* setup that produces downconversion. When classical light is used as input, only a small part of the incident power is converted into a correlated two-photon output field [21–23]. In chiral waveguides, however, it has been argued that two photons can be generated when one and only one photon is scattered in a C3LS structure [24]. Other downconversion mech-

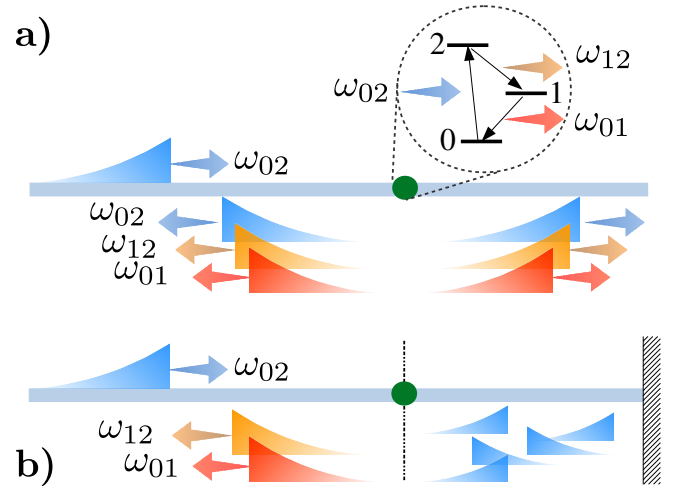


FIG. 1. (Color online) Downconversion setup. (a) A single incoming photon interacts with the three-level system. Part of it is transmitted/reflected (ω_{02} , blue) and part is downconverted into a pair of photons with frequencies ω_{12} and ω_{01} (orange and red). (b) Placing a mirror right after the scatterer at a suitable distance, downconversion can become deterministic: all reflected photons have downconverted frequencies.

anisms at the single photon limit, requiring the driving of nonlinear cavities, has been recently proposed [25]. In this paper we generalize the results in C3LS, considering full downconversion efficiency in non chiral waveguides. More precisely, we consider a waveguide photon impinging on the C3LS and resonantly populating level $|2\rangle$, as schematically represented in Fig. 1. Additionally to the direct relaxation of $|2\rangle$ to the ground state, the cascade $|2\rangle \rightarrow |1\rangle \rightarrow |0\rangle$ allows the relaxation to be accompanied by the emission of two photons [26]. In our study we include losses, analyze the entanglement of the output field and suggest a possible experimental realization.

The rest of the paper is organized as follows. In the next section, we introduce the model. Then, in Sect. III we sketch a realization in circuit QED. We continue by

reporting our numerical results, based on matrix product states (MPS). There, we discuss the two photon probability and the dynamics both for the field and the atom. We also characterize the output field and its entanglement. In Sect. V we develop an analytical theory, which allows to compute the efficiency in presence of losses [Sect. VI]. We conclude with the conclusions and send some technical issues to three appendices.

II. MODEL

We consider a cyclic three level quantum system (C3LS) strongly coupled to a one-dimensional waveguide where photons can freely travel. We neglect thermal fluctuations and losses in the waveguide and, for the moment in the C3LS, so the effective Hamiltonian is ($\hbar = 1$)

$$H = H_0 + H_{\text{int}}, \quad (1)$$

where

$$H_0 = \int d\omega \omega r_\omega^\dagger r_\omega + \int d\omega \omega l_\omega^\dagger l_\omega + \sum_{j=0}^2 \omega_j |j\rangle \langle j|, \quad (2)$$

with r_ω and l_ω being bosonic operators that, respectively, annihilate right- and left- moving waveguide photons; r_ω^\dagger and l_ω^\dagger are the corresponding creation operators, and ω_j and $|j\rangle$ are the eigenenergies and eigenstates of the isolated 3LS. The coupling between the 3LS and the waveguide photons is represented by $H_{\text{int}} = G X$, with X the electromagnetic (EM) displacement given by

$$X = \int d\omega D(\omega) (r_\omega + l_\omega) + \text{H.c.} \quad (3)$$

where $D(\omega)$ is the density of states. The operator G accounts for the transitions between levels in the C3LS induced by the EM field:

$$G = g_{01} |0\rangle \langle 1| + g_{12} |1\rangle \langle 2| + g_{02} |0\rangle \langle 2| + \text{H.c.} \quad (4)$$

III. A POSSIBLE IMPLEMENTATION

An important point is that a C3LS cannot be realized in systems where (i) quantum states are labelled by a spatial parity tag and (ii) are small enough and the dipolar interaction dominates (like atoms). The reason is that at least two of the three states in the C3LS must have the same parity, but the dipole interaction only couples states with different parity. However, effective C3LSs may appear in extended quantum systems, where couplings beyond the dipolar must be considered. Implementations of C3LS are some molecules [27] and flux qubits made of superconducting circuits [21, 22]. However, this last system leads to three quite dissimilar excitation energies. We chose an alternative design for an effective C3LS in

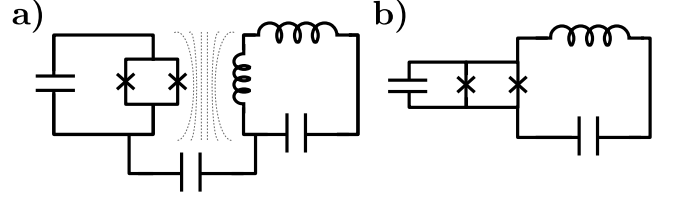


FIG. 2. (a) A transmon can be both inductively and capacitively coupled to an LC resonator. Coupling strength can be increased by either increasing the SQUID area or (b) by sharing a conductor segment, in the spirit of Ref. [29] and similar proposals.

the microwave range using a transmon (a charge superconducting qubit shunted by a big capacitor) that makes the C3LS transitions more harmonic [28].

Typically, inductive coupling between the transmon and the transmission line is negligible. The reason is that the transmon design is basically that of a one-dimensional electric dipole, without support for currents. In addition to this, the SQUID that controls the transmon frequency is small and shielded away from any coupling with the transmission line. Inductive couplings between transmons have been however demonstrated [30, 31]. We make use of similar ideas to envision a different coupling architecture that allows breaking the parity symmetry in the transmon setup.

Our starting point is a setup such as the one in Fig. 2a, where the transmon SQUID is no longer screened and the superconducting island couples both capacitively and inductively to the resonator. The circuit Lagrangian (with inductive and capacitive coupling) is,

$$\mathcal{L} = \int dx c (\partial_t \phi(x, t))^2 - \frac{1}{l} (\partial_x \phi(x, t))^2 + \frac{1}{2C_\Sigma} (q - \mathcal{Q})^2 - E_J \cos(2\pi \Phi / \Phi_0) \cos \varphi. \quad (5)$$

The first line accounts for the transmission line Lagrangian. Here, $\phi(x, t)$ is the (quantum) flux field, that in the interaction picture reads,

$$\phi(x, t) = \sqrt{\frac{\hbar Z_0}{4\pi}} \int_0^\infty d\omega \frac{1}{\sqrt{\omega}} \left(r_\omega e^{-i\omega(t-x/v)} + l_\omega e^{-i\omega(t+x/v)} + \text{H.c.} \right), \quad (6)$$

with c (l), the capacitance (inductance) per unit length and $Z_0 = \sqrt{l/c}$ is the line impedance. The transmon and its coupling is written in the second line. There, E_J is the Josephson energy and C_Σ is the capacitance. Charge and phase invariant gauge are quantized via $[e^{i\varphi}, q] = 2e e^{i\varphi}$. The transmon is driven and coupled to the line via the charge \mathcal{Q} and the flux Φ ($\Phi_0 = h/2e$ is the flux quantum):

$$\mathcal{Q} = 2e n_g + c \partial_t \phi(x, t) \quad (7)$$

$$\Phi = \lambda \partial_x \phi(x, t) + \frac{\Phi_0}{2\pi} \varphi_{\text{ext}}. \quad (8)$$

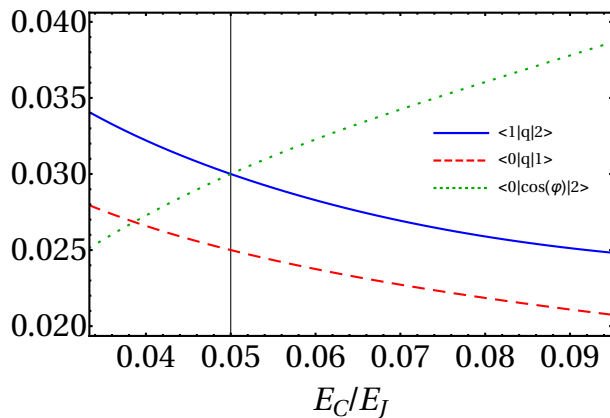


FIG. 3. (Color online) Non zero charge and flux matrix elements $\langle i|q|j\rangle$ and $\langle i|\cos\varphi|j\rangle$ respectively contributing to the coupling operator G . The vertical line marks the parameters chosen in our simulations with $E_C/E_J = 1/20$.

We have introduced the coupling factor λ that accounts for the effective field by the transmon's SQUID after taking into account the screening. Inserting the latter in (5) and expanding the cosine we get the coupling Hamiltonian,

$$H_{\text{coupling}} = \frac{c}{C_\Sigma} q \partial_t \phi - \lambda d \frac{\pi}{\Phi_0} E_J \sin(\varphi_{\text{ext}}) \cos(\varphi) \partial_x \phi. \quad (9)$$

We still need to show that (9) provides the cyclic structure. We numerically diagonalize $H_{\text{transmon}} = \frac{1}{2C_\Sigma} q^2 - E_J \cos\varphi$ in the charge basis, retaining the first three levels $H_{\text{transmon}} = \sum_{j=0}^2 \omega_j |j\rangle\langle j|$. With the eigenstates at hand, we can compute the different contributions to G in H [Eq. (1) in the main text]. In Figure 3 we plot the contributions due to the charge operator q in (9). As already explained in the literature, $\langle i|q|i+1\rangle \neq 0$ but $\langle 0|q|2\rangle = 0$ [28]. The necessary non zero g_{02} value is obtained through the inductive coupling. The values for $\langle 0|\cos(\varphi)|2\rangle \neq 0$ is also plotted in 3 ($\langle i|\cos(\varphi)|i+1\rangle = 0$). Therefore, by combining inductive and capacitive (electric and magnetic) coupling the transmon has a cyclic structure. Through the main text we set $E_C/E_J = 1/20$. We fix λ and C_Σ making the transition rates between quantum levels induced by coupling to the waveguide photons, $\Gamma_{ij}^{(0)} \equiv 2\pi D^2(\omega_{ij}) g_{ij}^2$, optimal for the two photon generation (see below).

IV. NUMERICAL SOLUTION

We compute the time evolution of an initial single-photon wavepacket. Even though, the results are independent of the actual wavepacket, our numerical simulations assume the incident photon being generated via spontaneous emission in an auxiliary two level system (a single photon generator). Besides, we discretize both space and time and use the Matrix Product States (MPS)

technique, which is a well known method for obtaining the ground state and low energy states in interacting one-dimensional systems [29, 32–35]. MPS has been applied to photon scattering in waveguides [19, 36, 37]. This method is specially suited for Hamiltonians like (2) that either have a nonlinear dispersion relation or, as in the considered case, do not conserve the number of excitations. It is worth to emphasize here that we solve the time evolution for the full Hamiltonian. As a consequence, we have access to both field and system observables at any time. Technical details of our simulations can be found in App. C.

A. Two photon generation: scattering and dynamics

In Fig. 4 we plot the spectrum for the one photon transmittance and reflectance, $|t^{(1)}(\omega)|^2 = \lim_{t \rightarrow \infty} |\langle \Omega | r_\omega e^{-iHt} | \psi_{\text{in}} \rangle| / |\langle \Omega | r_\omega | \psi_{\text{in}} \rangle|^2$ and $|r^{(1)}(\omega)|^2 = \lim_{t \rightarrow \infty} |\langle \Omega | l_\omega e^{-iHt} | \psi_{\text{in}} \rangle| / |\langle \Omega | r_\omega | \psi_{\text{in}} \rangle|^2$, respectively, and the total energy radiated in the two-photon channel $P^{(2)}(\omega)$. The first transmission dip occurs when the photon energy is centered around $\omega = \omega_{01} \equiv \omega_1 - \omega_0$. In this spectral region the $|0\rangle \rightarrow |1\rangle$ is the only transition available. Thus, the C3LS behaves as an effective two-level system and the photon is fully reflected at resonance [13–15]. Consequently, $P^{(2)}(\omega) = 0$ in this frequency range [Cf. Fig. 4 c)]. In the second transmission dip, located at $\omega = \omega_{02}$, the transmittance presents a finite minimum value, that is close to 0.5. Figs. 4 b)-c) shows a remarkable 50% downconversion efficiency of the incoming photon into just two (and only two) outgoing photons, with only a very small amount of light being backreflected.

For the shake of completeness and to emphasize the fact that we have access to the time domain too, we plot the 3CLS level population in Fig. 5 a). We see that the second excited state gets populated first, since our incident photon is resonant with the transition $|0\rangle \leftrightarrow |2\rangle$. After the transient period, both levels decay to the ground state. We also plot the particles in energy space, $\langle n_\omega^{(r)} \rangle = \langle r_\omega^\dagger r_\omega \rangle$ and similarly for $\langle n_\omega^{(l)} \rangle$ in Fig. 5 b) and c). In doing so, we can visualize the two photon generation in time domain. In the beginning, we have a single peak around the incident energy for the right-moving photons. After the interaction occurs, a peak appears for a left-moving photon at ω_{02} , corresponding to the single-photon reflection [See panel 5 c)]. In addition, two peaks emerge after the scattering for both forward and backward travelling photons centered at ω_{12} and ω_{01} , associated to the generation of the two-photon state.

B. Characterization for the two-photon output

In order to characterize the two-photon wave function emerging from the downconversion process we compute the two-point correlation function, both in position space

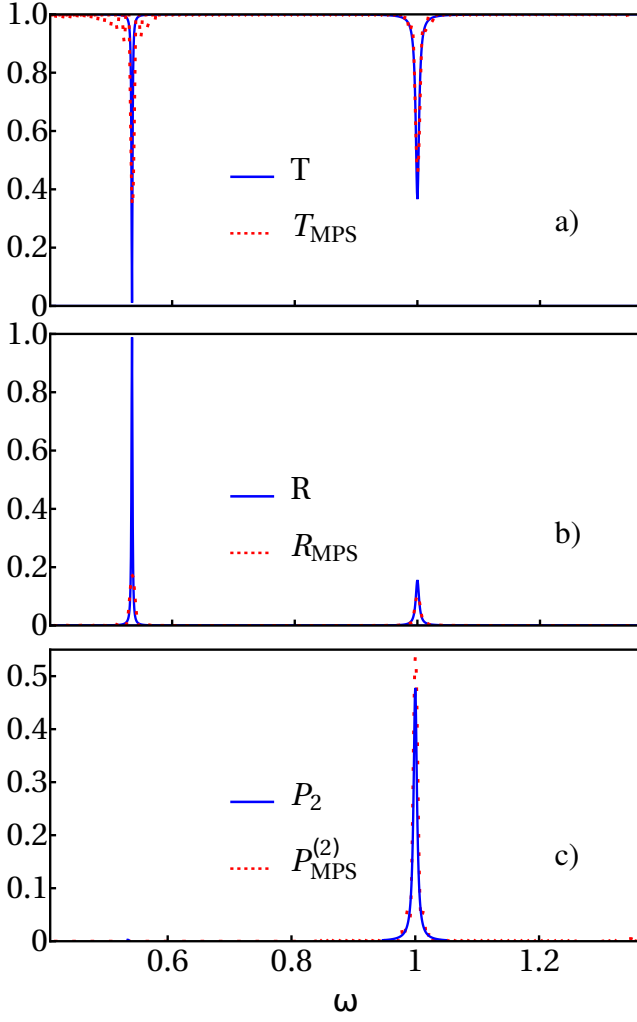


FIG. 4. (Color online). Scattering coefficients in a cyclic three-level system, as a function of the incident frequency ω . One photon transmittance (panel (a)), reflectance (panel (b)) and energy transferred into the two photon channel $P^{(2)}(\omega)$ (panel (c)). We show both analytical (solid lines) and numerical results obtained with MPS (dotted lines). The parameters are $\omega_{01} = 0.59$, $\omega_{02} = 1$, $\Gamma^{(0)}(\omega_{01}) = 1.7 \times 10^{-3}$, $\Gamma^{(0)}(\omega_{02}) = 2.3 \times 10^{-3}$ and $\Gamma^{(0)}(\omega_{12}) = 3.5 \times 10^{-3}$. We remind that $\Gamma_{ij}^{(0)} = 2\pi D^2(\omega_{ij})g_{ij}^2$.

$\phi_{x_1 x_2}^{\text{out}} := \langle \Omega | a_{x_1} a_{x_2} | \Psi(t_{\text{out}}) \rangle$, where a_x annihilates a photon at x and in energy space for right-moving photons $\tilde{\phi}_{\omega_1 \omega_2}^{\text{out}} := \langle \Omega | r_{\omega_1} r_{\omega_2} | \Psi(t_{\text{out}}) \rangle$. As shown in Fig. 6, both photons are emitted spatially in a symmetric way with respect to the position of the scatterer ($x = 0$). In energy space, $\tilde{\phi}_{\omega_1 \omega_2}^{\text{out}}$ is centered around $(\omega_1, \omega_2) = (\omega_{01}, \omega_{12})$ and $(\omega_{12}, \omega_{01})$ (white dotted lines), as expected from emission from a double resonant process. However, and similarly to the phenomena of resonant fluorescence, $\tilde{\phi}_{\omega_1 \omega_2}^{\text{out}}$ is non-zero all along the isoenergetic curve $\omega_1 + \omega_2 = \omega$ (white solid line in the panel b).

The two photons generated are entangled. The corresponding von Neumann entropy S_{VN} can be computed af-

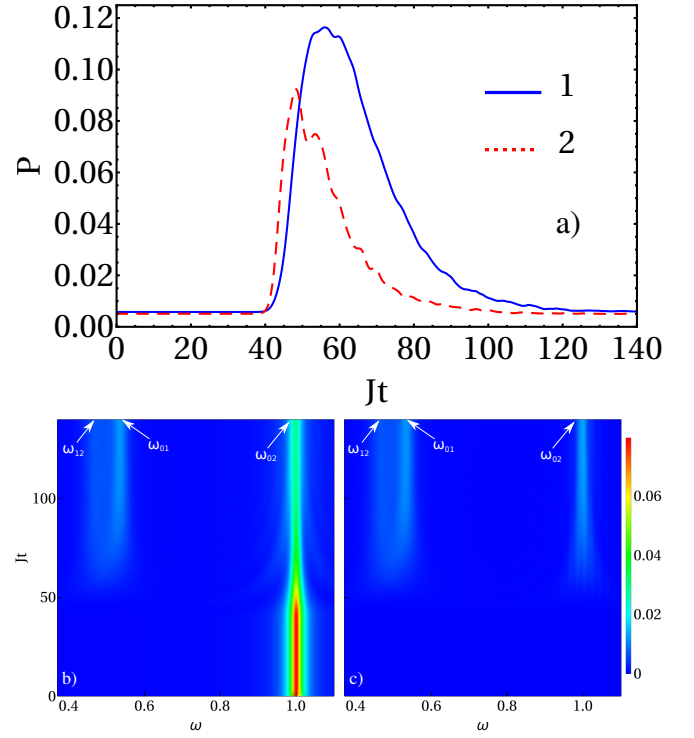


FIG. 5. (Color online) a) Population of the first (blue solid line) and second (red dashed line) excited states as a function of time. Photon occupation in energy space for b) right-moving, $\langle n_{\omega}^{(r)} \rangle$, and c) left-moving photons, $\langle n_{\omega}^{(l)} \rangle$, respectively, as a function of time. Same parameters as in Fig. 4.

ter normalizing the two-photon wave function, such that $\sum_{x_1 x_2} |\phi_{x_1 x_2}^{\text{out}}|^2 = 1$, and finding its Schmidt decomposition, $\phi_{x_1 x_2}^{\text{out}} = \sum_m \lambda_m \varphi_{x_1, m} \chi_{x_2, m}$, being $\{\lambda_m\}$ the singular values. Then $S_{\text{VN}} = -\sum_m \lambda_m^2 \log(\lambda_m^2)$ [38]. In the representative case shown in Fig. 6 we get $S_{\text{VN}} = 1.44$. For a better understanding, we plot the contribution of each mode to S_{VN} in Fig. 7 a). The entropy is dominated by the first two modes, but the contribution from the other modes is non negligible. In order to quantify how the entropy is recovered from a given number of modes, we define the entanglement entropy of the first m modes

$$S_{\text{VN}, m} = -\sum_{n=1}^m \lambda_n^2 \log(\lambda_n^2), \quad (10)$$

and show $S_{\text{VN}, m}/S_{\text{VN}}$ in the inset of Fig. 7.

Another measure of how the wavefunction can be represented by a fixed number of modes is the fidelity, *i.e.* the overlap between the actual two photon state, $|\Psi_2\rangle = 1/\sqrt{2} \sum_{x_1, x_2} \phi_{x_1, x_2} a_{x_1}^\dagger a_{x_2}^\dagger |\Omega\rangle$ and the state reconstructed with m modes:

$$|\Psi_{2, m}\rangle = \frac{1}{\sqrt{2}} \sum_{x_1, x_2} \sum_{n=1}^m \lambda_n \tilde{\varphi}_{x_1, n} \tilde{\chi}_{x_2, n} a_{x_1}^\dagger a_{x_2}^\dagger |\Omega\rangle. \quad (11)$$

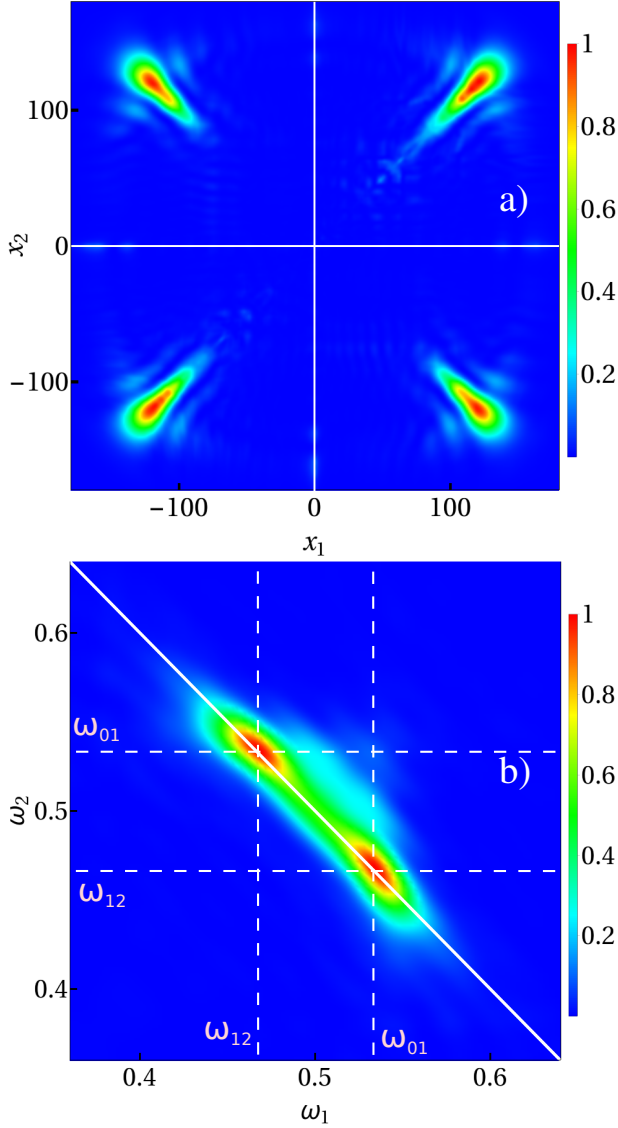


FIG. 6. (Color online) Square modulus of the two-photon wave function in a) position and b) energy space. The isoenergetic line, $\omega_1 + \omega_2 = \omega$, is shown in the bottom panel (white line). We normalize both wave functions such that $\max(|\phi_{x_1 x_2}^{\text{out}}|^2) = \max(|\phi_{\omega_1 \omega_2}^{\text{out}}|^2) = 1$. Same parameters as in Fig. 4.

In Fig. 7 a) (inset) we check that the overlap qualitatively behaves as $S_{VN,m}$.

Lastly, we can visualize how the two-point correlation function is reconstructed by adding modes. In Fig. 7 we plot $|\tilde{\phi}_{\omega_1, \omega_2}^m|^2 = |\langle \Omega | r_{\omega_1} r_{\omega_2} | \Psi_{2,m} \rangle|^2$ for different values of m . The white lines, as in Fig. 6, mark the isoenergetic condition. For $m = 1$ we do not catch the bimodal aspect of the state. However, already with $m = 2$ we see the double-peaked structure.

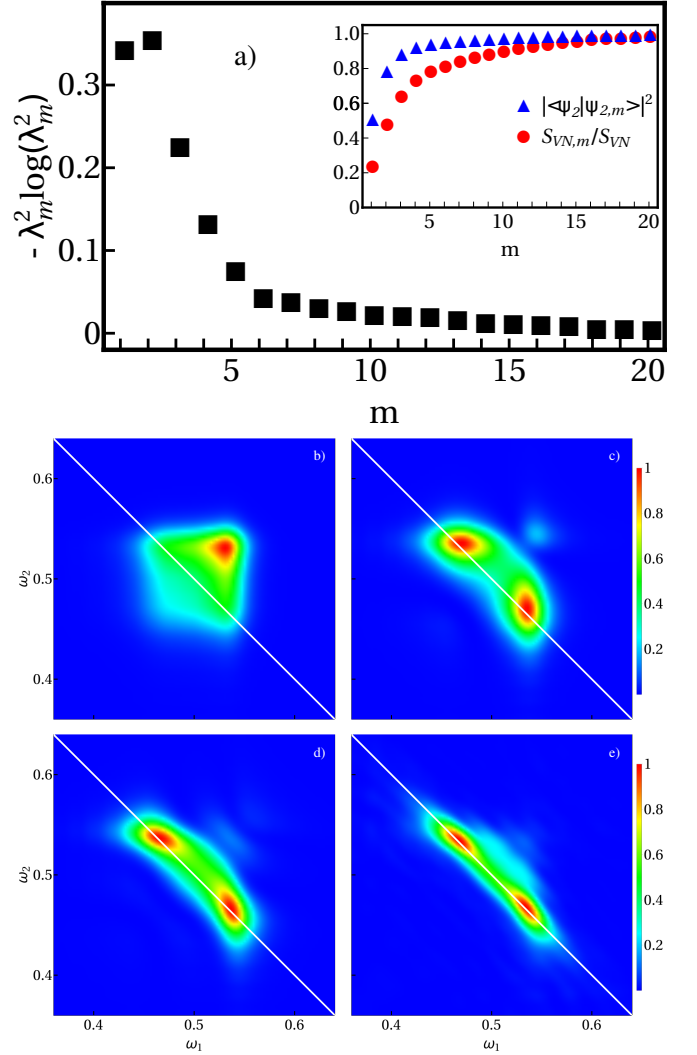


FIG. 7. (Color online) a) Contribution of each mode to S_{VN} , $-\lambda_m^2 \log(\lambda_m^2)$ as a function of m . In the inset, we plot the entropy of $|\Psi_{2,m}\rangle$ over the whole entropy, $S_{VN,m}/S_{VN}$ (red circles) and the overlap between $|\Psi_2\rangle$ and $|\Psi_{2,m}\rangle$ (blue triangles) as a function of m . $|\tilde{\phi}_{\omega_1, \omega_2}^m|^2$ for b) $m = 1$, c) $m = 2$, d) $m = 3$ and e) $m = L$ which is the exact result, Cf. Fig. 6b).

V. ANALYTICAL THEORY

In order to provide an approximate analytical theory for the numerical results presented above, we use the input-output formalism [39] that has been recently introduced to scattering problems in Waveguide QED [40, 41]. The central object in this theory is the relation among the input and output fields, namely,

$$r_{\text{out}}(t) = r_{\text{in}}(t) - i\sqrt{2\pi}D(\omega)G(t), \quad (12)$$

defined as $r_{\text{in}}(t) := \int_0^\infty \frac{d\omega}{\sqrt{2\pi}} r_\omega(t_0) e^{-i\omega t}$ and $r_{\text{out}}(t) := \int_0^\infty \frac{d\omega}{\sqrt{2\pi}} r_\omega(t_f) e^{-i\omega(t-t_f)}$ with $r_\omega(t) = e^{iHt} r_\omega e^{-iHt}$. The times t_0 and t_f must be taken well before and after the scattering event has occurred. As we are interested in

asymptotic behavior, we can set $t_0 \rightarrow -\infty$ and $t_f \rightarrow \infty$. It is important to notice that, in general, the relation (A12) is obtained assuming that the atom spontaneous emission rates $\Gamma_{ij}^{(0)} = 2\pi D^2(\omega_{ij})g_{ij}^2$ are small compared to the bare atom transitions.

The crucial point, as expressed in Eq. (A12), is that the full photon dynamics can be obtained from that of the quantum scatterer by solving the quantum optical master equation [39] for the reduced density matrix of the C3LS:

$$\begin{aligned} \frac{d\rho}{dt} = & -i[H_0, \rho] - 2i\alpha D(\omega) \cos(\omega t)[G(t), \rho] \\ & + 2 \sum_{\omega_{ij}>0} \Gamma_{ij} \left(L_{ij} \rho L_{ij}^\dagger - \frac{1}{2} \{L_{ij}^\dagger L_{ij}, \rho\} \right), \end{aligned} \quad (13)$$

where $L_{ij} = |j\rangle\langle i|$ and Γ_{ij} are the transition rates between the discrete levels in the scatterer. Additionally to the transition rates induced by coupling to the waveguide photons this formulation allows us to consider the transitions γ_{ij} induced by coupling to other baths (as phonons or other components of the EM field). In this case, the total transition rate is $\Gamma_{ij} = \Gamma_{ij}^{(0)} + \gamma_{ij}$.

As stated above, we have numerically tested that no more than two photons are generated in the dynamics. Therefore, the two photon generation probability can be computed by energy conservation:

$$P^{(2)}(\omega) = 1 - |t^{(1)}(\omega)|^2 - |r^{(1)}(\omega)|^2 - A(\omega). \quad (14)$$

The one photon transmittance $t_1(\omega)$ is given by

$$t^{(1)}(\omega) = \lim_{\alpha \rightarrow 0} \frac{\langle \alpha_\omega | r_{\text{out}}(t) | \alpha_\omega \rangle}{\langle \alpha_\omega | r_{\text{in}}(t) | \alpha_\omega \rangle} \quad (15)$$

with $|\alpha_\omega\rangle = e^{\alpha r_{\text{in}}^\dagger(\omega) - \text{H.c.}} |\Omega\rangle$, being $r_{\text{in}}^\dagger(\omega)$ the Fourier transform of $r_{\text{in}}^\dagger(t)$. Thus, $t^{(1)}(\omega)$ can be obtained by solving (A13) within linear response theory. After some algebra, we get A

$$t^{(1)}(\omega) = 1 - \frac{i\Gamma_{01}^{(0)}}{(\omega - \omega_{01}) + i\Gamma_{01}} - \frac{i\Gamma_{02}^{(0)}}{(\omega - \omega_{02}) + i(\Gamma_{01} + \Gamma_{02})}. \quad (16)$$

In addition, $1 + r^{(1)}(\omega) = t^{(1)}(\omega)$.

The last term in (17) is the energy “absorbed” by the lossy channels, $A(\omega)$. Here, we consider a unique channel dissipating all the C3LS transitions. Around the two photon frequency generation $A(\omega)$ can be approximated,

$$A(\omega \cong \omega_{02}) = 2\gamma_{02} |r^{(1)}(\omega_{02})|^2 / \Gamma_{02} \quad (17)$$

The validity of these approximate analytical expressions is shown in Fig. 4, where they are compared to the numerical results for the “lossless” case $\gamma_{ij} = 0$.

VI. EFFICIENCY

Equation (17) allows for the search of optimal parameters for downconversion. The first observation is that

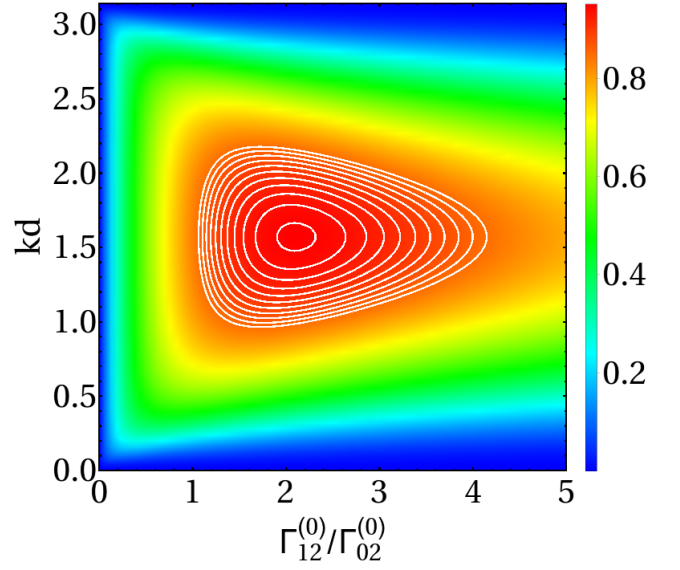


FIG. 8. (Color online) $P^{(2)}(\omega = \omega_{02})$ as a function of the distance atom-mirror kd , See Fig. 1, and the ratio $\Gamma_{12}^{(0)}/\Gamma_{02}^{(0)}$. Losses are taken into account. In the figure, a conservative ratio $\gamma_{02}/\Gamma_{02}^{(0)} = 0.1$ is used. The rest of the parameters are the same as in Fig. 4. White lines mark iso-efficiency curves, starting at 0.9 and finishing at 0.99.

losses are detrimental, always reducing $P^{(2)}(\omega)$. Even in absence of losses ($\gamma_{ij} = 0$), the two-photon generation can be considered as a loss mechanism *for the one-photon channel*, which implies that the fraction of energy down-converted is at most $\max P^{(2)}(\omega) = \frac{1}{2}$ (occurring when $r(\omega) = -\frac{1}{2}$). This fundamental bound is related to the fact that a deep subwavelength scatterer re-emits equally to the left and to the right [42]. But this bound can be exceeded by breaking the left-right symmetry in the waveguide by, *e.g.* placing a mirror next to the C3LS, as sketched in Fig. 1b).

The reflectance and (for $\gamma_{ij} \neq 0$) absorption can be calculated in this configuration by summing all multiple-scattering processes that the waveguide photon has with both the C3LS and the mirror [43]. The sum can be done analytically B, resulting in:

$$\begin{aligned} P^{(2)}(\omega) = & 1 - \left| \frac{r^{(1)}(\omega) - (1 + 2r^{(1)}(\omega))\Phi(\omega)}{1 + r^{(1)}(\omega)\Phi(\omega)} \right|^2 \\ & - \left| \frac{1 - \Phi(\omega)}{1 + r^{(1)}(\omega)\Phi(\omega)} \right|^2 A(\omega), \end{aligned} \quad (18)$$

where $\Phi(\omega) = e^{2ik(\omega)d}$, d is the distance between the mirror and the C3LS and $k(\omega)$ is the waveguide photon wavevector at frequency ω .

As drawn in Fig. 8, the maximum downconversion efficiency predicted by Eq. (18) occurs at resonance ($\omega = \omega_{02}$), and for $\Gamma_{12}^{(0)}/\Gamma_{02}^{(0)} \cong 2$ and $kd = \pi/2$, and can be

approximated by:

$$\max P_2 = 1 - \frac{\gamma_{02}}{\Gamma_{02}} \quad (19)$$

So, remarkably, downconversion may be perfect in the considered configuration if losses are negligible. It provides a simple expression for the maximum efficiency as a function of the ratio between the rates for absorption and coupling into waveguide photons. This ratio is a key figure of merit in Waveguide QED and values as small as 10^{-2} have already reported for effective two-level systems in both superconducting circuits [8] and photonic crystals [44]. Thus, two photon generation with one and only one photon with an efficiency larger than 0.99 is doable using an appropriate C3LS.

VII. CONCLUSIONS

We have shown that two photons can be efficiently generated by sending one and only one photon through a cyclic three-level atom in a realistic scenario. Remarkably, the downconversion process can occur with unit probability, being only limited by energy leakage in the three-level system. Based on reported experimental data, we have estimated that a nearly perfect two photon generator operating at the single photon level is feasible in architectures based on either photonic crystals or superconducting circuits. Together with single atomic mirrors [13–15], single photon lasing [16] or single photon Raman scattering [19], this work contributes to the toolbox of photonics with minimum power, where even tasks usually associated to high intensities are performed at the one-photon level.

ACKNOWLEDGMENTS

We acknowledge support by the Spanish Ministerio de Economía y Competitividad within projects MAT2014-53432-C5-1-R, FIS2012-33022 and FIS2014-55867-P, CAM Research Network QUITEMAD+ and the Gobierno de Aragón (FENOL group).

Appendix A: One photon scattering, input-output and Linear Response Theory

To start with, we define the S -matrix, as $S := \lim_{t \rightarrow \infty} U(t, -t)$ with $U(t, t') = e^{-iH(t-t')}$ the evolution operator. Then [40, 41]:

$$t^{(1)}(\omega) = \lim_{t \rightarrow \infty} \frac{\langle \Omega | r_{\omega} r_{\text{out}}^{\dagger}(t) | \psi_{\text{in}} \rangle}{\langle \Omega | r_{\omega} r_{\text{in}}^{\dagger}(t) | \psi_{\text{in}} \rangle}. \quad (A1)$$

The second equality holds after direct replacement of the definitions for the input output fields appearing in the

Gardiner and Collet seminal paper [39],

$$r_{\text{in}}(t) := \int_0^{\infty} \frac{d\omega}{\sqrt{2\pi}} r_{\omega}(t_0) e^{-i\omega(t-t_0)} \quad (A2)$$

$$r_{\text{out}}(t) := \int_0^{\infty} \frac{d\omega}{\sqrt{2\pi}} r_{\omega}(t_f) e^{-i\omega(t-t_f)} \quad (A3)$$

Here, $r_{\omega}(t) = e^{iHt} r_{\omega} e^{-iHt}$ are Heisenberg evolved operators. The times t_0 and t_f are times well before and well after the scatterer and the impinging photons have interacted. If we are interested in asymptotics, we can set $t_0 \rightarrow -\infty$ and $t_f \rightarrow \infty$.

Consider now a coherent input state,

$$|\alpha_{\omega}\rangle = e^{\alpha r_{\text{in}}^{\dagger}(\omega) - \text{H.c.}} |\Omega\rangle. \quad (A4)$$

We consider the following expected value

$$f_{\text{out}}(\omega, \omega', \alpha) := \langle \alpha_{\omega} | r_{\text{out}}(\omega') | \alpha_{\omega} \rangle, \quad (A5)$$

with $r_{\text{out}}(\omega)$ the Fourier transform of $r_{\text{out}}(t)$, Eq. (A3). We take a series expansion in α

$$f_{\text{out}}(\omega, \omega', \alpha) = \alpha \langle \Omega | r_{\text{out}}(\omega') r_{\text{in}}^{\dagger}(\omega) | \Omega \rangle + \mathcal{O}(\alpha^2) \quad (A6)$$

Following Fan et al. [40], $\langle \Omega | r_{\text{out}}(\omega') r_{\text{in}}^{\dagger}(\omega) | \Omega \rangle = t^{(1)}(\omega) \delta(\omega - \omega')$. Thus

$$f_{\text{out}}(\omega, \omega', \alpha) = \alpha t^{(1)}(\omega) \delta(\omega - \omega') + \mathcal{O}(\alpha^2). \quad (A7)$$

Fourier transforming with respect to ω'

$$f_{\text{out}}(\omega, t, \alpha) := \frac{1}{\sqrt{2\pi}} \int d\omega' f_{\text{out}}(\omega, \omega', \alpha) e^{i\omega' t} \quad (A8)$$

$$= \frac{\alpha}{\sqrt{2\pi}} t^{(1)}(\omega) e^{i\omega t} + \mathcal{O}(\alpha^2). \quad (A9)$$

Notice that $f_{\text{out}}(\omega, t, \alpha) = \langle \alpha_{\omega} | r_{\text{out}}(t) | \alpha_{\omega} \rangle$. Then, the transmission amplitude can be computed as

$$t^{(1)}(\omega) = \lim_{\alpha \rightarrow 0} \frac{\langle \alpha_{\omega} | r_{\text{out}}(t) | \alpha_{\omega} \rangle}{\langle \alpha_{\omega} | r_{\text{in}}(t) | \alpha_{\omega} \rangle} \quad (A10)$$

Therefore, the one photon scattering can be obtained by driving the scatterer with a coherent (classical) state in the limit of weak amplitude, α . Thus, Linear Response Theory can be used.

1. Input-output fields calculations

The exact relation between input and output fields, Eqs. (A2) and (A3) is [39]

$$r_{\text{out}}(t) = r_{\text{in}}(t) - i \int_0^{\infty} \frac{d\omega}{\sqrt{2\pi}} \int_{t_0}^{t_f} d\tau D(\omega) e^{-i\omega(t-\tau)} X(\tau). \quad (A11)$$

If we assume that the coupling to the line is small compared to the scatterer transitions, only photons close

to resonance (with such transitions) will actually interact with the scatterer. This is typical in experiments. Then, we can approximate the functional form $D(\omega)$ for its value at the incident photon frequency, ω , and (A11) is simplified:

$$r_{\text{out}}(t) = r_{\text{in}}(t) - i\sqrt{2\pi}D(\omega)G(t) \quad (\text{A12})$$

As a main consequence, $r_{\text{out}}(t)$ can be obtained by calculating the system dynamics. It turns out that, with the same assumption yielding (A12), $G(t)$ can be obtained through the quantum optical master equation [39],

$$\begin{aligned} \frac{d\rho}{dt} = & -i[H_{\text{sct}}, \rho] - ix(t)[G, \rho] \\ & + 2 \sum_{\omega_{ij}>0} \Gamma(\omega_{ij}) \left(L_{ij}\rho L_{ij}^\dagger - \frac{1}{2}\{L_{ij}^\dagger L_{ij}, \rho\} \right). \end{aligned} \quad (\text{A13})$$

where $L_{ij} = |j\rangle\langle i|$ and

$$\Gamma(\omega_{ij}) = 2\pi D^2(\Omega)g_{ij}^2 + \gamma_{ij} \quad (\text{A14})$$

Here, γ_{ij} are the decays to another environments. The (classical) driving, due to the coherent input state, enters in the second term of (A13). The driving due to the coherent input state (A4) is taken into account in the second term of (A13) via

$$x(t) = \langle X(t) \rangle_{\text{line}} = \text{Tr}(X(t)\rho_{\text{line}}(t_0)) \quad (\text{A15})$$

here, $X(t) = e^{iH_{\text{line}}t} X e^{-iH_{\text{line}}t}$, with $\rho_{\text{line}}(t_0)$ is the state of the line (already with the input state). In the case of a coherent state as input (A4),

$$x(t) = 2\alpha D(\omega) \cos(\omega t) \quad (\text{A16})$$

To solve for $t^{(1)}(\omega)$ [Cf. Eq. (15)] equation (A13) must be solved in the limit of weak driving: $\alpha \rightarrow 0$.

2. Linear Response theory (LRT)

We review the Linear Response Theory (LRT), See. e.g. Ref. 45, Chap. 6. We rewrite (A13) as,

$$\partial\rho = \mathcal{L}_0\rho + \lambda f(t)\mathcal{L}_1\rho \quad (\text{A17})$$

with,

$$\mathcal{L}_0\rho = -i[H_S, \rho] \quad (\text{A18})$$

$$+ 2 \sum_{\Omega} \Gamma(\Omega) \left(G(\Omega)\rho G^\dagger(\Omega) - \frac{1}{2}\{G^\dagger(\Omega)G(\Omega), \rho\} \right).$$

$$\mathcal{L}_1\rho = f(t)[G, \rho] \quad (\text{A19})$$

and,

$$\lambda = \alpha \sqrt{\left| \frac{d\omega}{dk} \right|} D(\omega) \quad f(t) = e^{-i\omega t}. \quad (\text{A20})$$

LRT solves the above evolution up to first order in λ :

$$\rho = \rho_0 + \lambda \rho_1 \quad (\text{A21})$$

with $\mathcal{L}_0\rho_0 = 0$, *i.e.* in absence of perturbation the system is in equilibrium. Replacing the above in (A17) we get (up to first order)

$$\partial_t \rho_1 = \mathcal{L}_0\rho_1 + f(t)\mathcal{L}_1\rho_0. \quad (\text{A22})$$

The solution ($\rho_1(-\infty) = 0$) is

$$\rho_1 = \int_{-\infty}^t ds e^{(t-s)\mathcal{L}_0} f(s) \mathcal{L}_1\rho_0. \quad (\text{A23})$$

The solution (A23) is used to compute averages. In particular the one for G :

$$\Delta G(t) := \langle G \rangle(t) - \langle G \rangle_0 \quad \langle G \rangle_0 \equiv \text{Tr}(G\rho_0), \quad (\text{A24})$$

obtaining,

$$\Delta G(t) = \lambda \int_{-\infty}^{\infty} ds R(t-s) f(s) \quad (\text{A25})$$

with the *response function* ($\theta(t) = 0$ if $t < 0$, $\theta(t) = 1$ otherwise)

$$R(t) = \theta(t) \text{Tr}(e^{(t-s)\mathcal{L}_0} \mathcal{L}_1\rho_0). \quad (\text{A26})$$

Importantly enough, the response function $R(t)$ does not depend on the actual form for $f(t)$.

3. Practical calculation

We discuss two important perturbation functions $f(t)$. We also give the relation between them.

a. Retarded perturbation

In the, so called retarded perturbation, the perturbation \mathcal{L}_1 switched off at $t = 0$. Therefore,

$$f_r(t) = \theta(-t) \quad (\text{A27})$$

In this case (A25)

$$\begin{aligned} \Delta G_r(t) &= \lambda \int_{-\infty}^{\infty} ds R(t-s) \theta(-s) \\ &= \lambda \int_{-\infty}^{\infty} ds R(s) \theta(s-t) \\ &= \lambda \int_t^{\infty} ds R(s) \longrightarrow \frac{d}{dt} \Delta G_r = -\lambda R(t) \end{aligned} \quad (\text{A28})$$

b. AC-driving

We consider now, the AC-driving $f(t) = e^{-i\omega t}$. In this case,

$$\begin{aligned}\Delta G_{\text{AC}}(t) &= \lambda \int_{-\infty}^{\infty} ds R(t-s) e^{-i\omega s} \\ &= \lambda e^{-i\omega t} \int_{-\infty}^{\infty} ds R(s) e^{i\omega s} \\ &= \lambda e^{-i\omega t} \int_0^{\infty} ds R(s) e^{i\omega s} \equiv \lambda G(\omega) e^{-i\omega t}.\end{aligned}\quad (\text{A29})$$

The last equality defines the susceptibility.

c. The relation

Finally, both results the AC susceptibility and the retarded evolution, Eqs. (A28) and (A29) can be related,

$$\begin{aligned}\Delta G_{\text{AC}}(t) &= -e^{-i\omega t} \left(\int_0^{\infty} ds \frac{d}{ds} \Delta G_{\text{r}} e^{i\omega s} \right) \\ &= -e^{-i\omega t} \left(\int_0^{\infty} ds \frac{dG_{\text{r}}}{ds} e^{i\omega s} \right) \\ &= e^{-i\omega t} \left(G_{\text{r}}(0) + i\omega \int_0^{\infty} ds G_{\text{r}}(s) e^{i\omega s} \right)\end{aligned}\quad (\text{A30})$$

Here $G_{\text{r}}(\infty) = 0$.

Summarizing, for computing the evolution under AC driving we do not need to solve the explicit time dependent problem (A17) but solve the unperturbed evolution with initial conditions $(\mathcal{L}_0 + \lambda \mathcal{L}_1)\varrho = 0$ (the retarded response).

4. Final formula

The solution for $\partial_t \varrho = \mathcal{L}_0 \varrho$ is

$$G_{\text{r}}(s) = \sum_{ij} G_{i,j} \varrho_{ij}(0) e^{-(i\omega_{ij} + \Gamma_{ij})s} \quad (\text{A31})$$

with $G_{i,j} = \langle i|G|j \rangle$ and $\varrho_{ij}(0)$ the initial conditions obtained by solving $(\mathcal{L}_0 + \lambda \mathcal{L}_1)\varrho = 0$. Eq. (A30) can be rewritten (and approximated) in energy space

$$\begin{aligned}\Delta G_{\text{AC}}(\omega) &= \sum_{ij} G_{i,j} \varrho_{ij}(0) \left(1 + \frac{i\omega}{i(\omega_{ij} - \omega) + \Gamma_{ij}} \right) \\ &= \sum_{ij} G_{i,j} \varrho_{ij}(0) \frac{i\omega_{ij} + \Gamma(\omega_{ij})}{i(\omega_{ij} - \omega) + \Gamma_{ij}} \\ &\cong \sum_{\omega_{ij} > 0} G_{i,j} \varrho_{ij}(0) \frac{i\omega_{ij} + \Gamma(\omega_{ij})}{i(\omega_{ij} - \omega) + \Gamma_{ij}}\end{aligned}\quad (\text{A32})$$

The last approximation considers that the main contribution comes from the terms with poles.

5. Transmission calculation

Following Eq. (A32), we can approximate

$$G_{\text{r}}(s) \cong G_{01} \varrho_{10}(0) e^{-(i\omega_{01} + \Gamma(\omega_{01}))s} + G_{02} \varrho_{20}(0) e^{-(i\omega_{02} + \Gamma(\omega_{02}))s} \quad (\text{A33})$$

Finally, we solve for $\varrho_{ij}(0)$, that are solutions of $(\mathcal{L}_0 + \lambda \mathcal{L}_1)\varrho = 0$. We get the equations,

$$\dot{\varrho}_{10} = 0 = -i\omega_{01} \varrho_{10} - i\alpha g_{10}(\varrho_{00} - \varrho_{11}) - \Gamma_{01} \varrho_{20} \quad (\text{A34})$$

$$\dot{\varrho}_{20} = 0 = -i\omega_{02} \varrho_{20} - i\alpha g_{20}(\varrho_{00} - \varrho_{22}) - (\Gamma_{02} + \Gamma_{01}) \varrho_{20} \quad (\text{A35})$$

and the ones for the diagonals

$$\dot{\varrho}_{00} = 0 = -i\alpha g_{10}(\varrho_{01} - \varrho_{10}) - i\alpha g_{20}(\varrho_{02} - \varrho_{20}) + \Gamma_{01} \varrho_{11} + \Gamma_{02} \varrho_{22} \quad (\text{A36})$$

$$\dot{\varrho}_{11} = 0 = +i\alpha g_{10}(\varrho_{01} - \varrho_{10}) - i\alpha g_{21}(\varrho_{12} - \varrho_{21}) - \Gamma_{01} \varrho_{11} + \Gamma_{12} \varrho_{22} \quad (\text{A37})$$

and $\varrho_{22} = 1 - \varrho_{11} - \varrho_{00}$. From (A36) and (A37) we see that, $\varrho_{11} \sim \varrho_{22} \sim \mathcal{O}(\alpha)$ and $\varrho_{00} \sim 1 - \mathcal{O}(\alpha)$ which makes trivial solve (A34) and (A35) up to first order in α . Inserting their solutions in the general expression (A32) we get the equation in main text.

6. Leakage

Losses can be modelled as decays to another channels. Here, we take into account one channel (others will sum

up), see Fig. 9. The input-output relations (A12) must

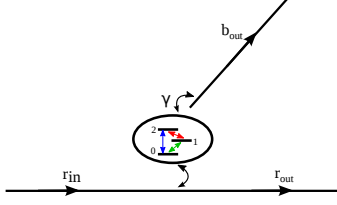


FIG. 9. (Color online) Schematics for the modeling of non-radiative losses

be generalized now to include this *extra* channel,

$$r_{\text{out}}(t) = r_{\text{in}}(t) - i\sqrt{2\pi}D(\omega)G(t) \quad (\text{A38})$$

$$b_{\text{out}}(t) = b_{\text{in}}(t) - i\sqrt{2\gamma}G(t). \quad (\text{A39})$$

The γ gives a phenomenological loss rate, and the 2 in front is because we do not consider left and right modes in the non radiative channel but just b -modes. Besides, $b_{\text{in}}(t) = 0$ and the transmission in the b -modes read,

$$\tau(\omega) = \frac{-i\sqrt{2\gamma}\langle G \rangle}{\langle r_{\text{in}} \rangle} \quad (\text{A40})$$

Appendix B: Efficiency calculations

In order to compute the reflection and leakage when the mirror is placed, we must sum over all the possible reflection, transmission and leakage events, as shown in Figure 10. In doing so, we name $\Phi(\omega) = \exp(ik(\omega)d)$ the phase accumulated by a photon with quasi momentum k travelling a distance d (this will be the distance between the mirror and the atom). Finally, we denote the reflection in the mirror as r_M . Eventually, we will set $r_M = -1$, *i.e.* we neglect losses in the mirror, which is a good experimental assumption.

With the mirror, $P_2(\omega)$ is written as,

$$P_2(\omega) = 1 - |r_{\text{tot},1}(\omega)|^2 - |\tau_{\text{tot}}(\omega)|^2 \quad (\text{B1})$$

where $r_{\text{tot},1}(\omega)$ is the *total* one photon reflection. It should be distinguished from r_1 which stands for the reflection occurring in every event. Finally, $\tau_{\text{tot}}(\omega)$ is the total leakage. Summing over all the events, see Figure 10, we finally get

$$\begin{aligned} r_{\text{tot},1}(\omega) &= r_1(\omega) + t^{(1)}(\omega)\Phi(\omega)r_M t^{(1)}(\omega) \\ &\quad + t^{(1)}(\omega)\Phi(\omega)r_M t^{(1)}(\omega)r_1(\omega)\Phi(\omega)r_M t^{(1)}(\omega) + \dots \\ &= r_1(\omega) + \frac{(t^{(1)}(\omega))^2 \Phi(\omega) r_M}{1 - r_1(\omega)\Phi(\omega)r_M}, \end{aligned} \quad (\text{B2})$$

and

$$\begin{aligned} \tau_{\text{tot}}(\omega) &= \tau(\omega) + t^{(1)}(\omega)\Phi(\omega)r_M \tau(\omega) \\ &\quad + t^{(1)}(\omega)\Phi(\omega)r_M t^{(1)}(\omega)r_1(\omega)\Phi(\omega)r_M \tau(\omega) + \dots \\ &= \tau(\omega) + \frac{\tau(\omega)t^{(1)}(\omega)\Phi(\omega)r_M}{1 - r_1(\omega)\Phi(\omega)r_M}. \end{aligned} \quad (\text{B3})$$

Combining (B2), (B3) with (B1) we can compute the two photon generation $P^{(2)}(\omega)$, considering $r_M = -1$. In the main text, we introduce

$$A(\omega) \equiv |\tau(\omega)|^2. \quad (\text{B4})$$

Appendix C: Numerical simulations

1. Matrix Product States

We are studying the dynamics of a state with one or two photons flying over the ground state, *i.e.* the state is expected to have a small amount of entanglement. Therefore, we can use the variational ansatz of Matrix Product States [34, 35] to describe the discrete wave function as we have shown recently [19, 36]. This ansatz has the form

$$|\psi\rangle = \sum_{s_x \in \{1, d_x\}} \text{tr} \left[\prod A_x^{s_x} \right] |s_1, s_2, \dots, s_L\rangle. \quad (\text{C1})$$

It is constructed from L sets of complex matrices $A_x^{s_x} \in M[\mathbb{C}^D]$, with L the number of sites, where each set is labelled by the quantum state s_x of the corresponding site. The local Hilbert space dimension d_x is infinity, since we are dealing with bosonic sites. During the dynamics, processes that create more than two photons are still highly off-resonance. In consequence, we can truncate the bosonic space and consider states with 0 to n_{max} photons per cavity. The composite Hilbert space is $\mathcal{H} = \bigotimes_x \mathbb{C}^{d_x}$, where the dimension is $d_x = n_{\text{max}} + 1$ for the empty resonators and $d_{x_0} = 3(n_{\text{max}} + 1)$ for the cavity with the three-level system. We thus expect the composite wave function of the photon-C3LS to consist of a superposition with a small number of photons

The total number of variational parameters $(L - 1)D^2(n_{\text{max}} + 1) + 3D^2(n_{\text{max}} + 1)$ depends on the size of the matrices, D . The key point is that, for describing a general state, D increases exponentially with L , whereas it increases polynomially if the entanglement is small enough.

Our work with MPS uses four different algorithms. The most basic one is to create product states such as a vacuum state with the deexcited C3LS: $|\psi\rangle = |0\rangle|\text{vac}\rangle$. These states can be reproduced using matrices of bond dimension $D = 1$, so each matrix is just a coefficient $A_x^{s_x} = \delta_{s_x,1}$. The second algorithm is to compute expectation values from MPS. This amounts to a contraction of tensors that can be performed efficiently [34], and allows us to compute single-site operators $\langle a_x^\dagger a_x \rangle$, $\langle \sigma_z \rangle$, correlators as $\langle a_x^\dagger a_x \rangle$ or even projections as $\langle \Omega | a_{x_1} a_{x_2} | \psi \rangle$. The third operation that we need to perform is to apply operators on to the state, $O|\psi\rangle$, such as introducing or removing excitations $a_x^\dagger |\psi\rangle$. We do this in an efficient fashion by interpreting the operator O as a Matrix Product Operator (MPO) [46]. A MPO is a matrix product representation of an operator:

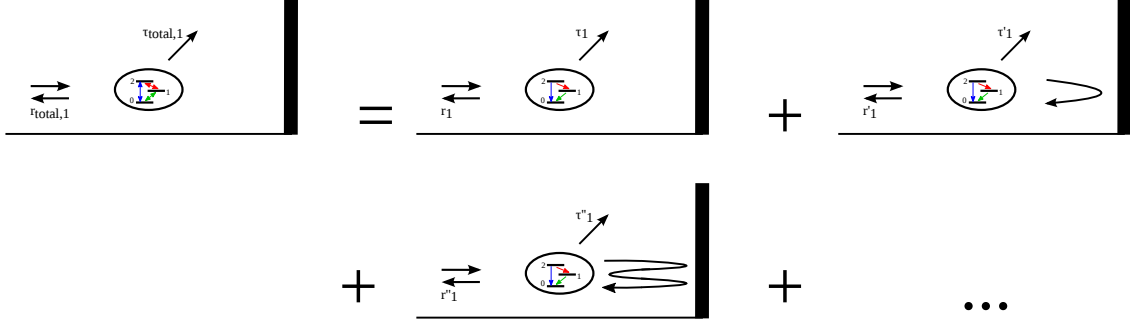


FIG. 10. (Color online) Diagrammatic plot for the possible scattering events giving the total reflection

$$O = \sum_{s_x, s'_x \in \{1, d_x\}} \text{tr} \left[\prod B_x^{s_x, s'_x} \right] |s_1, s_2, \dots, s_L\rangle \langle s'_1, s'_2, \dots, s'_L| \quad (\text{C2})$$

So, now we have L sets of complex matrices $B_x^{s_x, s'_x} \in M[\mathbb{C}^{D_O}]$, where each set is labelled by two indices s_x, s'_x of the corresponding site.

We just need to apply sums of one-body operators

$$O = a_\phi^\dagger = \sum_x \phi_x a_x^\dagger. \quad (\text{C3})$$

In such a case, an efficient representation of the MPO is obtained with $D_O = 2$

$$B_x^{s_x, s'_x} = \begin{pmatrix} \delta_{s_x, s'_x} & 0 \\ \phi_x (a_x^\dagger)_{s_x, s'_x} & \delta_{s_x, s'_x} \end{pmatrix} \quad x = 2, 3, \dots, L-1, \quad (\text{C4})$$

whereas $B_1^{s_1, s'_1} = (\phi_1 (a_1^\dagger)_{s_1, s'_1}, \delta_{s_1, s'_1})$ and $B_L^{s_L, s'_L} = (\delta_{s_L, s'_L}, \phi_L (a_L^\dagger)_{s_L, s'_L})^T$, with $(a_x^\dagger)_{s_x, s'_x} =: \langle s_x | a_x^\dagger | s'_x \rangle$.

Finally, we can also approximate time evolution, repeatedly contracting the state with an MPO approximation of the unitary operator $\exp(-iH\Delta t)$ for short times, and truncating it to an ansatz with a fixed D . Since our problem does not contain long-range interactions and since the state is well approximated by MPS, it is sufficient to rely on a third-order Suzuki-Trotter formula [47]. In the same way as we can consider time evolution, we can take imaginary time to obtain the ground state, that is solving the equation $\frac{d}{dt} |\psi\rangle = -H |\psi\rangle$ for finite time-steps, while constantly normalizing the state. Provided a suitable initial state, the algorithm converges to the lowest-energy state of H . Notice that the ground state is totally necessary to study the dynamics, since our initial state is obtained by applying a single-body operator as that of Eq. C3 over the ground state.

2. Simulated model, input state and parameters used

For the photonic medium, we consider a one-dimensional array of coupled cavities:

$$H = \epsilon \sum_x a_x^\dagger a_x - J \sum_x (a_x^\dagger a_{x+1} + \text{H.c.}) \quad (\text{C5})$$

$$+ \sum_i \omega_i |i\rangle \langle i| + \sum_{ij} (g_{ij} |i\rangle \langle j| + \text{H.c.}) (a_0 + a_0^\dagger),$$

being ϵ the bare frequencies of the cavities, J the hopping between nearest neighbours and g_{ij} the coupling constant for the $|i\rangle \leftrightarrow |j\rangle$ transition. The lattice spacing d is fixed to 1. The photonic part can be diagonalized in momentum space, giving the dispersion relation $\omega(k) = \epsilon - 2J \cos k$. The density of electromagnetic modes will be $D(\omega) = 1/\sqrt{2J|\sin(k(\omega))|}$.

We fix $\epsilon = 1$, $J = 1/\pi$, $\omega_0 = 0$, $\omega_1 = 0.59$ and $\omega_2 = 1.10$ (these energies were obtained from the model introduced in the main part of the text). We take $L = 1000$ cavities and we place the scatterer at $x_0 = 500$ (in the main text, we consider $x_0 = 0$). The couplings used in the simulations to compute the full spectrum are $g_{01} = -0.0225$, and $g_{12} = g_{02} = 0.03$, which were obtained from the physical implementation we shall explain below. In the simulations in which we computed the two-photon wave function, in order to get a cleaner scattering state and due to limitations in the time of simulation, we artificially increased the couplings: $g_{01} = -0.10$, $g_{12} = g_{02} = 0.13$.

We work in position space. The input state is:

$$|\Psi_{\text{in}}\rangle = \sum_x e^{ik_0 x} e^{(x-\bar{x})/2\sigma} \theta(x_0 - x) a_x^\dagger |\Omega\rangle, \quad (\text{C6})$$

up to a normalization constant, with \bar{x} the position of the wave front, σ the width, k_0 the mean momentum

and $\theta(x)$ the Heaviside function. We fix $\bar{x} = 420$ and $k_0 = 1.73$ (on resonance with ω_{02}). We take $\sigma = 2$ for the simulations to get the full spectrum and $\sigma = 20$ for the simulation in which we compute the two-photon

wave function. The results reported used bond dimension $D = 10$ and the cut-off for the cavities is $n_{\max} = 3$. We checked that these sizes are already sufficient.

-
- [1] O. Astafiev, A. M. Zagoskin, A. A. Abdumalikov, Y. A. Pashkin, T. Yamamoto, K. Inomata, Y. Nakamura, and J. S. Tsai, *Science* **327**, 840 (2010).
 - [2] I. C. Hoi, C. M. Wilson, G. Johansson, T. Palomaki, B. Peropadre, and P. Delsing, *Phys. Rev. Lett.* **107**, 073601 (2011).
 - [3] I.-C. Hoi, A. F. Kockum, T. Palomaki, T. M. Stace, B. Fan, L. Tornberg, S. R. Sathyamoorthy, G. Johansson, P. Delsing, and C. M. Wilson, *Phys. Rev. Lett.* **111**, 053601 (2013).
 - [4] A. F. van Loo, A. Fedorov, K. Lalumière, B. C. Sanders, A. Blais, and A. Wallraff, *Science (New York, N.Y.)* **342**, 1494 (2013).
 - [5] I.-C. Hoi, C. M. Wilson, G. Johansson, J. Lindkvist, B. Peropadre, T. Palomaki, and P. Delsing, *New Journal of Physics* **15**, 025011 (2013).
 - [6] D. Reitz, C. Sayrin, R. Mitsch, P. Schneeweiss, and A. Rauschenbeutel, *Phys. Rev. Lett.* **110**, 243603 (2013).
 - [7] J. D. Thompson, T. G. Tiecke, N. P. de Leon, J. Feist, A. V. Akimov, M. Gullans, A. S. Zibrov, V. Vuletić, and M. D. Lukin, *Science (New York, N.Y.)* **340**, 1202 (2013).
 - [8] M. Arcari, I. Söllner, A. Javadi, S. Lindskov Hansen, S. Mahmoodian, J. Liu, H. Thyrrstrup, E. Lee, J. Song, S. Stobbe, and P. Lodahl, *Phys. Rev. Lett.* **113**, 093603 (2014).
 - [9] R. Yalla, M. Sadgrove, K. P. Nayak, and K. Hakuta, *Phys. Rev. Lett.* **113**, 143601 (2014).
 - [10] A. Goban, C.-L. Hung, S.-P. Yu, J. D. Hood, J. A. Muniz, J. H. Lee, M. J. Martin, A. C. McClung, K. S. Choi, D. E. Chang, O. Painter, and H. J. Kimble, *Nature Communications* **5**, 3808 (2014).
 - [11] P. Lodahl, S. Mahmoodian, and S. Stobbe, *Reviews of Modern Physics* **87**, 347 (2015).
 - [12] A. Javadi, I. Söllner, M. Arcari, S. L. Hansen, L. Midolo, S. Mahmoodian, G. Kiršansk, T. Pregnolato, E. H. Lee, J. D. Song, S. Stobbe, and P. Lodahl, (2015), arXiv:1504.06895.
 - [13] J.-T. Shen and S. Fan, *Optics Letters* **30**, 2001 (2005).
 - [14] J.-T. Shen and S. Fan, *Phys. Rev. Lett.* **95**, 213001 (2005).
 - [15] L. Zhou, Z. R. Gong, Y. xi Liu, C. P. Sun, and F. Nori, *Phys. Rev. Lett.* **101**, 100501 (2008).
 - [16] E. Rephaeli and S. Fan, *Phys. Rev. Lett.* **108**, 143602 (2012).
 - [17] K. Koshino, K. Inomata, T. Yamamoto, and Y. Nakamura, *Phys. Rev. Lett.* **111**, 153601 (2013).
 - [18] K. Inomata, K. Koshino, Z. R. Lin, W. D. Oliver, J. S. Tsai, Y. Nakamura, and T. Yamamoto, *Phys. Rev. Lett.* **113**, 063604 (2014).
 - [19] E. Sánchez-Burillo, D. Zueco, J. J. García-Ripoll, and L. Martín-Moreno, *Phys. Rev. Lett.* **113**, 263604 (2014).
 - [20] R. W. Boyd, *Nonlinear Optics, Second Edition*, 2nd ed. (Academic Press, 2003).
 - [21] Y.-x. Liu, J. Q. You, L. F. Wei, C. P. Sun, and F. Nori, *Phys. Rev. Lett.* **95**, 087001 (2005).
 - [22] Y.-x. Liu, H.-C. Sun, Z. H. Peng, A. Miranowicz, J. S. Tsai, and F. Nori, *Scientific Reports* **4**, 7289 (2014).
 - [23] S. R. Sathyamoorthy, A. Bengtsson, P. Delsing, and G. Johansson, (2015), arXiv:1511.03038.
 - [24] K. Koshino, *Phys. Rev. A* **79**, 013804 (2009).
 - [25] Y. Chang, A. González-Tudela, C. Sánchez-Muñoz, C. Navarrete-Benlloch, and T. Shi, , 14 (2015), arXiv:1510.07307.
 - [26] M. O. Scully and M. S. Zubairy, *Quantum Optics* (Cambridge University Press, 1997).
 - [27] P. Král and M. Shapiro, *Phys. Rev. Lett.* **87**, 183002 (2001).
 - [28] J. Koch, T. Yu, J. Gambetta, A. Houck, D. Schuster, J. Majer, A. Blais, M. Devoret, S. Girvin, and R. Schoelkopf, *Phys. Rev. A* **76**, 042319 (2007).
 - [29] B. Peropadre, D. Zueco, D. Porras, and J. J. García-Ripoll, *Phys. Rev. Lett.* **111**, 243602 (2013).
 - [30] Y. Chen, C. Neill, P. Roushan, N. Leung, M. Fang, R. Barends, J. Kelly, B. Campbell, Z. Chen, B. Chiaro, A. Dunsworth, E. Jeffrey, A. Megrant, J. Y. Mutus, P. J. J. O'Malley, C. M. Quintana, D. Sank, A. Vainsencher, J. Wenner, T. C. White, M. R. Geller, A. N. Cleland, and J. M. Martinis, *Phys. Rev. Lett.* **113**, 220502 (2014).
 - [31] É. Dumur, B. Küng, A. K. Feofanov, T. Weissl, N. Roch, C. Naud, W. Guichard, and O. Buisson, *Phy. Rev. B* **92**, 020515 (2015).
 - [32] G. Vidal, *Phys. Rev. Lett.* **91**, 147902 (2003).
 - [33] G. Vidal, *Phys. Rev. Lett.* **93**, 040502 (2004).
 - [34] J. J. García-Ripoll, *New Journal of Physics* **8**, 305 (2006).
 - [35] F. Verstraete, V. Murg, and J. I. Cirac, *Advances in Physics* **57**, 143 (2008).
 - [36] E. Sánchez-Burillo, J. García-Ripoll, L. Martín-Moreno, and D. Zueco, *Faraday discussions* **178**, 335 (2015).
 - [37] T. Ramos, B. Vermersch, P. Hauke, H. Pichler, and P. Zoller, (2016), arXiv:1602.00926.
 - [38] R. Pāškauskas and L. You, *Phys. Rev. A* **64**, 042310 (2001).
 - [39] C. Gardiner and M. Collett, *Phys. Rev. A* **31**, 3761 (1985).
 - [40] S. Fan, Şükrü Kocabaş, and J.-T. Chen, *Phys. Rev. A* **82**, 063821 (2010).
 - [41] S. Xu and S. Fan, *Phys. Rev. A* **91**, 043845 (2015).
 - [42] B. Peropadre, G. Romero, G. Johansson, C. M. Wilson, E. Solano, and J. J. García-Ripoll, *Phys. Rev. A* **84**, 063834 (2011).
 - [43] Eventually, we will set $r_M = -1$, *i.e.* we neglect losses in the mirror, wich is a good experimental assumption.
 - [44] I. Söllner, S. Mahmoodian, S. L. Hansen, L. Midolo, A. Javadi, G. Kiršansk, T. Pregnolato, H. El-Ella, E. H. Lee, J. D. Song, S. Stobbe, and P. Lodahl, *Nature Nanotechnology* **10**, 775 (2015).
 - [45] J. L. Garcia-Palacios, , 104 (2007), arXiv:0701242 [cond-mat].

- [46] B. Pirvu, V. Murg, J. Cirac, and F. Verstraete, New Journal of Physics **12**, 025012 (2010).
- [47] M. Suzuki, Journal of Mathematical Physics **32**, 400 (1991).